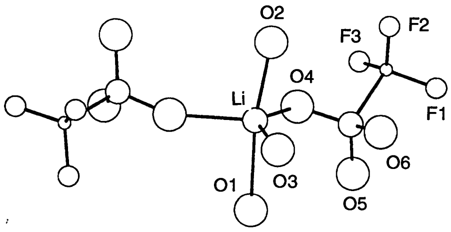

Fig. 4. Local environment around Li^+, showing coordination by three ether oxygens and oxygens from two neighboring triflate groups.

with the phase diagram study of Vallée, Besner, and Prud'homme (*12*). Several earlier reports have suggested stoichiometries of PEO_4:$LiCF_3SO_3$ or $PEO_{3.5}$:$LiCF_3SO_3$ (*13*). This would require partial occupancy of the Li/CF_3SO_3 sites in our model. In order to explore the stoichiometry, we fixed the temperature factors for the Li/CF_3SO_3 species at 0.08 Å^2. After refinement, the occupancy value was 0.96(1), which sets an upper limit on the PEO:$LiCF_3SO_3$ ratio of 3.13(3). We can reasonably conclude that there is no significant deviation from the ideal 3:1 stoichiometry. The latter two possible explanations for the high thermal parameters were explored by carrying out low-temperature refinements. The relatively smooth variation of U_{iso} versus temperature observed for F and O suggests that this phenomenon is associated merely with thermal and not static disorder. The relatively large displacements (0.10 Å) for F even at low temperature are not surprising and may be expected from the very weak coordination of this part of the complex.

Results of the Rietveld refinement for the room-temperature structure are given in Tables 1 and 2. The final model consisted of 113 variables refined against 2600 data points and 88 soft constraints. The data range covered was $8° < 2\theta < 60°$ (Fig. 1). Final agreement factors were $R_{wp} = 3.84\%$ and $\chi^2 = 1.83$. Views of the structure along *b* and *c* are given in Figs. 2 and 3, respectively. The helical arrangement of the PEO chain within the unit cell is similar to that for the previously determined 3:1 complexes, NaSCN (*5*), NaI (*6*), and $NaClO_4$ (*7*). However, the disposition of the inorganic portion of the structure relative to this is significantly different than in the previous cases, reflecting the different size and shape of the anion and the smaller size of the cation. Focusing on one PEO chain (Figs. 2 and 3), the Li^+ ions are located within it, forming a zigzag pattern along the axis of the helix (that is, *b*). Lithium is coordinated by five oxygens, composed of three PEO oxygens and one oxygen from each of two different $CF_3SO_3^-$ groups (Figs. 3 and 4). The coordination is best described as trigonal bipyramidal, with the three PEO oxygens being almost coplanar. Each $CF_3SO_3^-$ group associated with the chain bridges two adjacent Li^+ ions, one oxygen being coordinated to each lithium, leaving the third oxygen free. There is little interchain interaction, the $-CF_3$ groups being located in the space between the chains. The crystal structure demonstrates strikingly that these compounds are columnar coordination complexes, with long chains of Li^+ ions being coordinated by ether oxygens and triflate anions (Fig. 2), the solid polymer results from chain entanglement rather than any ionic cross-linking. It is also evident from the crystal structure that replacement of the $-CF_3$ group with a bulkier, preferably asymmetric group, would inhibit crystallization. This is presumably the origin of the wide range of amorphicity exhibited by PEO:Li[$(CF_3SO_2)_2N$] and PEO:Li[$(CF_3SO_2)_3C$].

REFERENCES AND NOTES

1. D. E. Fenton, J. M. Parker, P. V. Wright, *Polymer* **14**, 589 (1973).
2. M. B. Armand, J. M. Chabagno, M. Duclot, in *Fast Ion Transport in Solids*, P. Vashista, J. M. Mundy, G. K. Shenoy, Eds. (North-Holland, Amsterdam, 1979), p. 131.
3. J. R. MacCallum and C. A. Vincent, Eds., *Polymer Electrolyte Reviews* (Elsevier, London, 1989), vols. 1 and 2.
4. F. M. Gray, *Solid Polymer Electrolytes: Fundamentals and Technological Applications* (VCH Press, Cambridge, United Kingdom, 1991).
5. Y. Chatani and S. Okamura, *Polymer* **28**, 1815 (1987).
6. Y. Chatani, Y. Fujii, T. Takayanagi, A. Honma, *ibid.* **31**, 2238 (1990).
7. P. Lightfoot, M. A. Mehta, P. G. Bruce, *J. Mater. Chem.* **2**, 379 (1992).
8. Powder x-ray diffraction data were collected on a Stoe STADI/P system (equipped with a position-sensitive detector covering ~6° in 2θ) with monochromatized $CuK_{\alpha 1}$ radiation. The sample was mounted in a 0.5-mm Lindemann tube, and data were collected over the range $8° < 2\theta < 60°$ and at temperatures between 100 and 298 K. Low-temperature runs were performed with an Oxford Cryostream system.
9. P.-E. Werner, *Z. Kristallogr.* **120**, 375 (1964).
10. Coordinates for the PEO part of the structure were used directly from Chatani's refinement, with the addition of hydrogen atoms in idealized positions. Because of the differing cell size, the coordinates of the atoms in the chain had to be adjusted to produce an idealized PEO chain conforming to the known "*trans-trans-gauche*" conformation (*5*). Soft (chemical) constraints on both bond lengths and angles were used in order to optimize this geometry, namely C–O = 1.44(1) Å, C–C = 1.57(1) Å, and C–H = 1.09(1) Å (errors in the last digit given in parentheses), with tetrahedral angles at 109° and C–C and C–O torsion angles at 60° and 180°, respectively.
11. A. C. Larson and R. B. Von Dreele, *Los Alamos Natl. Lab. Rep. No. LA-UR-86-748* (1987).
12. A. Vallée, S. Besner, J. Prud'homme, *Electrochim. Acta* **37**, 1579 (1982).
13. P. R. Sorensen and T. Jacobsen, *Polym. Bull.* **9**, 47 (1983); C. Berthier *et al.*, *Solid State Ionics* **11**, 91 (1983).

14. P.G.B. is indebted to the Royal Society for the award of a Pickering Research Fellowship and to SERC for financial support.

7 June 1993; accepted 7 September 1993

Fire History and Climate Change in Giant Sequoia Groves

Thomas W. Swetnam

Fire scars in giant sequoia [*Sequoiadendron giganteum* (Lindley) Buchholz] were used to reconstruct the spatial and temporal pattern of surface fires that burned episodically through five groves during the past 2000 years. Comparisons with independent dendroclimatic reconstructions indicate that regionally synchronous fire occurrence was inversely related to yearly fluctuations in precipitation and directly related to decadal-to-centennial variations in temperature. Frequent small fires occurred during a warm period from about A.D. 1000 to 1300, and less frequent but more widespread fires occurred during cooler periods from about A.D. 500 to 1000 and after A.D. 1300. Regionally synchronous fire histories demonstrate the importance of climate in maintaining nonequilibrium conditions.

Despite the complexity inherent in local fire regimes, regional fire activity often oscillates in phase with year-to-year climatic variability. For example, the area burned annually across the southern United States tends to decrease during El Niño years and increase during La Niña years (*1*). This coupling between wildland fire and climate raises the possibility that intrinsic and stochastic factors, while contributing to local ecosystem heterogeneity, are overridden by regional climatic events and trends. Rapid, regional changes in vegetation may result from extreme climate-linked disturbances, such as catastrophic crown fires, whereas relatively slow vegetation changes may follow gradual, climate-driven shifts in surface-fire regimes (*2*). A broad range of spatial and temporal observations is therefore necessary to distinguish local- from regional-scale patterns and to encompass both high- and low-frequency changes in processes (*3*).

A commonly observed but rarely quantified phenomenon of disturbance regimes is

Laboratory of Tree-Ring Research, University of Arizona, Tucson, AZ 85721.

a tendency for disturbance intensity and size to be inversely related to disturbance frequency (4). For example, large, high-intensity crown fires tend to occur in forests with low fire frequency, and relatively small, low-intensity surface fires tend to occur in forests with high fire frequency (5). Traditionally, these heterogeneous fire regimes were thought to result from complex interactions of local-scale patterns of water balance, topography, soils, succession, and fuel dynamics (5). Asynchronous fire histories would be expected among widely dispersed forest stands if past fire regimes had been dominated by the local-scale processes. However, if fire events were significantly in phase at regional scales then large-scale climatic processes were dominant in controlling fire regimes. I analyzed spatial and temporal fire-regime changes at local-to-regional and annual-to-millennial scales by reconstructing a set of 1500- to 2000-year fire histories in five giant sequoia groves of the Sierra Nevada, California. Combined with dendroclimatic reconstructions of winter-spring precipitation (6, 7) and summer temperatures (7, 8), these data provide multi-scale perspectives of climate-fire dynamics.

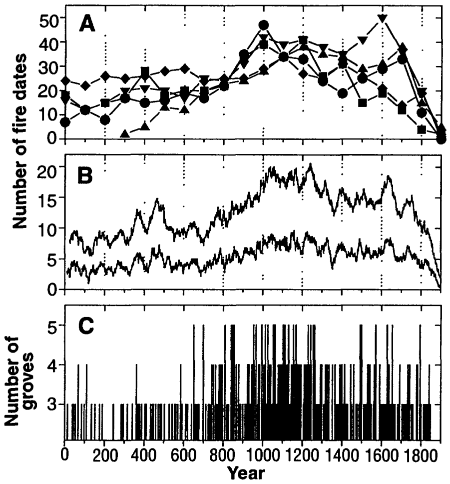

Fig. 1. (**A**) Fire frequency computed as the number of fires per century in each of the five sequoia groves since 1 B.C. The frequencies are plotted on the first year of the indicated century. Symbols: triangles, Mariposa; diamonds, Mountain Home; upside-down triangles, Big Stump; squares, Giant Forest; circles, Atwell. (**B**) Fire frequency computed as the number of fires occurring in 50-year (top trace) and 20-year (bottom trace) moving windows. Combined fire dates from all five groves are included. The frequencies are plotted on the central year (25th and 10th years, respectively) of the moving periods. (**C**) Synchronous fire events in three, four, and five groves are plotted as vertical lines.

Giant sequoias grow at mid-elevations (about 1800 to 2300 m) on the western slope of the Sierra in about 75 disjunct groves (9). The five sampled groves are distributed along a 160-km transect from Yosemite National Park in the north to Sequoia National Park and Mountain Home State Forest in the south (Mariposa, Big Stump, Giant Forest, Atwell, and Mountain Home groves). The five groves are sufficiently isolated that fire spread from one grove to another is unlikely. Other conifer tree species in the groves included white fir (*Abies concolor*), red fir (*Abies magnifica*), sugar pine (*Pinus lambertiana*), ponderosa pine (*Pinus ponderosa*), and incense cedar (*Calocedrus decurrens*).

I sampled 16 to 29 dead sequoia trees (stumps, logs, and snags) in each grove for a total of 90 sampled trees. The sampled trees were distributed throughout areas ranging from 13 to 69 ha. More than 500 partial cross sections were obtained with chainsaws from ground level inside deep fire-scar cavities at the base of the trees. The sections were sanded with belt sanders, and all tree rings were exactly dated by cross-dating (matching of ring-width patterns) (10). Dates (in years) of past fires were determined by observing the location of the fire-caused lesions (fire scars) within annual rings. Short-term ring growth surges (growth releases) that were closely associated with the fire scars were also used to date past fires (11).

Giant sequoia tree rings contain long and well-preserved fire records. The oldest dated fire occurred in 1125 B.C., but rec-

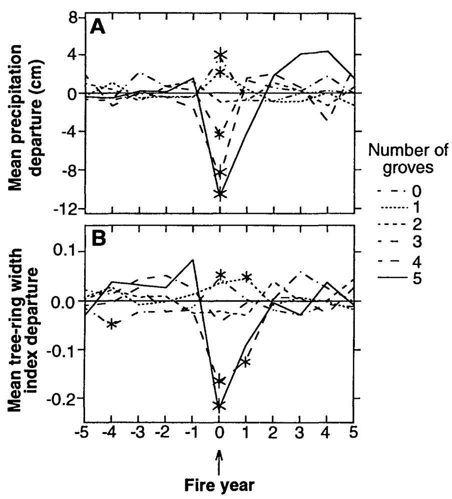

Fig. 2. (**A**) Tree-ring reconstructed, winter-spring precipitation (6) departures from the mean (A.D. 1060 to 1850) during fire years (lag year 0) and the years lagged before and after the fire years. The fire years were sorted by their recorded occurrence in one to five groves (1 grove, 242 events; 2 groves, 149 events; 3 groves, 114 events; 4 groves, 56 events; 5 groves, 20 events). The set of nonfire years (no fires recorded in any of the groves) was also tested (0 groves, 214 events). Significance levels were estimated from confidence intervals derived from a bootstrap procedure, in which the same number of key years was randomly selected in 1000 trials (small asterisks, $P < 0.01$; large asterisks, $P < 0.001$). (**B**) A similar analysis carried out with a precipitation-responsive, bristlecone pine tree–ring chronology (A.D. 500 to 1850) from the White Mountains, California (7) (0 groves, 448 events; 1 grove, 434 events; 2 groves, 232 events; 3 groves, 173 events; 4 groves, 80 events; 5 groves, 33 events).

Table 1. Synchrony of fires per century in five giant sequoia groves. Expected (Ex) and observed (Ob) numbers of fires co-occurring in different combinations of groves are shown.

Century	Number of co-occurring fire dates*												Total† χ^2
	0 Groves		1 Grove		2 Groves		3 Groves		4 Groves		5 Groves		
	Ex	Ob	Ex	Ob	Ex	Ob	Ex	Ob	Ex	Ob	Ex	Ob	
500	34.9	41	40.9	33	19.2	17	4.5	8	0.5	1	0.0	0	5.9
600	34.0	42	40.9	34	19.7	13	4.7	9	0.6	0	0.0	2	11.3‡
700	30.0	44	40.8	31	22.2	6	6.1	12	0.8	7	0.0	0	41.8§
800	26.7	40	40.4	31	24.4	14	7.4	7	1.1	4	0.1	4	18.1§
900	16.3	27	35.7	31	31.2	19	13.6	12	3.0	8	0.3	3	14.6‖
1000	9.9	20	29.1	29	34.2	16	20.1	21	5.9	9	0.7	5	22.5§
1100	11.6	29	31.2	27	33.6	14	18.1	9	4.9	12	0.5	9	39.9§
1200	10.4	17	29.8	35	34.1	19	19.5	11	5.6	14	0.6	4	12.2‖
1300	17.3	24	36.4	32	30.6	23	12.9	14	2.7	7	0.2	0	6.7
1400	17.5	24	36.5	33	30.4	20	12.7	17	2.6	4	0.2	2	9.9‡
1500	19.6	28	37.8	31	29.1	23	11.2	11	2.2	6	0.2	1	7.6
1600	16.1	23	35.5	33	31.3	19	13.8	20	3.0	3	0.3	2	11.6‖
1700	21.3	32	38.6	28	28.0	21	10.1	14	1.8	4	0.1	1	13.9‖
1800	47.0	57	38.3	26	12.5	8	2.0	8	0.2	1	0.0	0	28.7§
Total	312.8	448	511.9	434	380.4	232	156.7	173	34.9	80	3.3	33	

*The "0 Grove" category includes numbers of dates when no fires were recorded in any grove. Expected values were estimated from joint probabilities of fire (or no fire) occurring within the groves (13). †The 3, 4, and 5 grove categories were combined to achieve expected cell frequencies greater than 5.0—a necessary condition of this test. The expected number of 3, 4, and 5 grove events for the 1800s, however, was still only 2.2, so the χ^2 value for this period is suspect. ‡$P < 0.05$. §$P < 0.001$. ‖$P < 0.01$.

ords in most sampled trees extended back to about A.D. 500. An average of 63.8 fire dates was recorded per sampled tree. Even low-intensity surface fires burning up to the base of sequoia trees often radiate sufficient heat to kill living tissue along the edges of old fire-scar cavities where the bark is relatively thin. Because of the low flammability of sequoia wood and resin, repeated fires usually do not burn off the lesions (scars) caused by older fires. Many replicated observations of the same fire dates recorded on different samples from the same trees, and on different trees of varying age and size, demonstrate the consistency and reliability of the fire-scar record. Furthermore, there was excellent agreement between known fire dates from the late 1800s to the present and the fire record based on tree rings.

Shifts in fire frequency and synchrony within and among the groves were apparent at time scales of centuries, decades, and years (Fig. 1). All groves sustained lower fire frequencies from about the A.D. 500s to 800. Fire frequency (within groves) during these centuries ranged from 13 to 29 fires per century. Fire frequency increased regionally after about 800, and fire frequencies were highest in four of the five sampled groves from approximately 1000 to 1300. Fire frequencies during this period ranged from 27 to 46 fires per century. Fire frequencies generally declined after about 1300, except for a short episode of increased fire frequency during the 1600s in one grove (Big Stump) and the 1700s in three groves (Big Stump, Mariposa, and Atwell). The longest fire-free intervals lasted from 15 to 30 years during the low fire-frequency periods, whereas during the 1000 to 1300 period the longest fire-free intervals were always less than 13 years. All fire chronologies showed greatly reduced fire occurrence after about 1860. This sharp decline in regional burning was probably a result of intensive sheep grazing, a decrease in fires set by Native Americans, and fire suppression by government agencies (*12*).

In addition to the general similarity of long-term fire-frequency patterns among the groves (Fig. 1A), year-to-year fire occurrence was highly synchronous (Fig. 1C). I used a contingency analysis to estimate the statistical significance of the observed fire synchrony. Expected numbers of co-occurring fire dates among the five groves were estimated from the joint probabilities of fire occurrence in all combinations of two, three, four, and five groves (*13*). The co-occurrence of the same fire years in multiple groves and the co-occurrence of years when no fires occurred in any of the groves (non-fire years) was much higher than would be expected to occur by chance during most centuries (Table 1). Climate is the most likely cause of such a synchronized pattern among widely dispersed sites.

Comparison of the fire years and non-fire years with tree-ring estimates of past precipitation (*6, 7*) confirms that multiple-grove fire events tended to occur during dry years (Fig. 2). A similar year-to-year comparison with temperature estimates (*7, 8*) did not show any statistically significant patterns ($P > 0.05$). Years when fires were recorded in three, four, or five groves were increasingly dry, whereas years when no fires were recorded in any of the groves were wet. This result suggests that the extensiveness of fire and non-fire years was associated with the magnitude of winter-spring rainfall fluctuations.

Decadal-to-centennial fluctuations in growing season temperatures generally matched similar long-term variations in regional-scale fire activity (Fig. 3 and Table 2). The long-term variations in the precipitation time series (not shown), however, had no significant association with changes in fire frequency (Table 2). Thus, precipitation was most important to fire occurrence at time scales of years (Fig. 2), whereas summer temperature was most important at time scales of decades to centuries (Fig. 3). I propose that these frequency-dependent climate-fire patterns were a result of (i) extreme, short-term (high-frequency) changes in precipitation-related fuel moisture changes and (ii) long-term (low-frequency) temperature-related shifts in vegetation and in the production of fuels (*14*).

The fire-scar record also reveals the importance of fuel accumulation processes at the geographically local scale. The combined record indicates that some fires probably burned throughout individual groves and some fires were smaller and burned only around a single tree or group of trees. The estimates of fire frequency and fire extent in

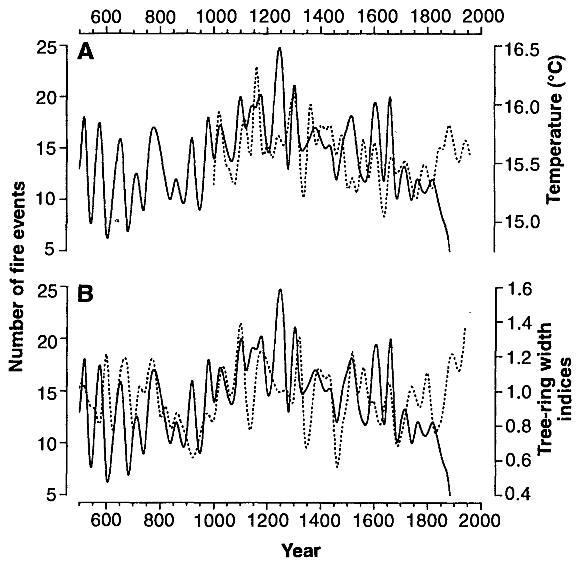

Fig. 3. (**A**) Long-term variations in tree-ring reconstructed summer (June to August) temperature (dotted trace) (*8*) (A.D. 1000 to 1990) compared with regional fire occurrence (solid trace) in giant sequoia groves. Twenty-year nonoverlapping means of the temperatures, slightly smoothed with a cubic spline, were used in the graphical comparison to emphasize decadal-scale trends. The fire time series was the sum of the weighted fire events occurring in each 20-year period. For example, a fire date recorded in five groves had a value of 5, a four-grove fire date had a value of 4, and so on. Thus, both regional fire frequency and synchrony are reflected in this time series. (**B**) A similar comparison with temperature-responsive bristlecone pine from the White Mountains (A.D. 500 to 1970) (tree-ring–width indices, dotted trace; fire occurrence, solid trace) (*7*).

Table 2. Correlations between regional fire occurrence in giant sequoia groves and tree-ring reconstructed summer temperature [Sum temp (*8*)]; tree-ring reconstructed winter-spring precipitation [WS precip (*6*)]; upper forest border, bristlecone pine tree-ring–width indices [BCP temp, inferred temperature record (*7*)]; and lower forest border, bristlecone pine tree-ring–width indices (BCP precip, inferred precipitation record (*7*)]. Each time series was composed of sequential 20-year nonoverlapping means. The pearson correlation (*r*), probability level (*P*), number of 20-year data points (*n*), and time period tested (period) is listed for each combination. The shorter time periods corresponding to the length of the reconstructions and the longer time period encompassed by the bristlecone pine tree-ring–width chronologies are indicated (STP and LTP, respectively).

	Sum temp	BCP temp (STP)	WS precip	BCP precip (STP)	BCP temp (LTP)	BCP precip (LTP)
r	.414	.362	−.171	−.066	.302	−.066
P	.006	.017	.290	.684	.012	594
n	43	43	40	40	68	68
Period	1000 to 1850	1000 to 1850	1060 to 1850	1060 to 1850	500 to 1850	500 to 1850

the groves apparently have a nonlinear relation (Fig. 4A). The exponential shape of this relation suggests that the relative size of fires enlarged at an increasing rate as the average interval between fires lengthened. My interpretation is that during periods of high fire frequency the fuels were maintained at low levels, resulting in a patchy pattern of smaller fires and perpetuating an uneven distribution (a fine-grain spatial pattern) of vegetation and fuels. During periods of low fire frequency, more fuels accumulated and the resulting fires were more widespread and intense, producing a more homogeneous distribution of vegetation and fuels (a coarse-grain spatial pattern).

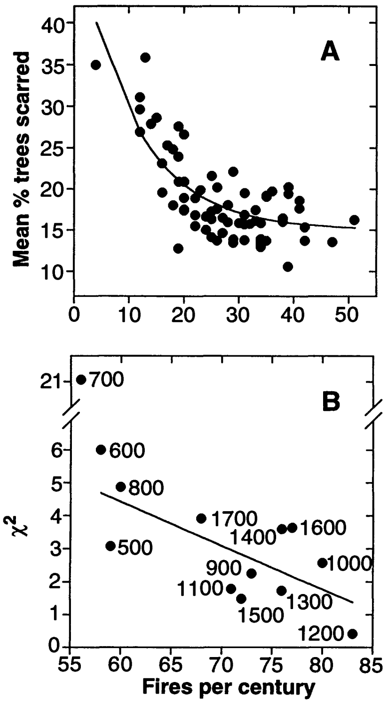

Fig. 4. (**A**) Fire extent versus fire frequency within the groves. The centennial fire frequencies from all groves (A.D. 500 to 1850) are plotted against the mean percentage of trees recording individual fires in each corresponding century in each grove. Percentages of trees recording fires are inferred to be estimates of relative fire extent within the sampled areas. (**B**) A similar inverse pattern of fire frequency and extent at larger spatial scales. In this case, fire synchrony among multiple groves is taken as a proxy of regional fire extensiveness. Here, the measure of fire synchrony is the χ^2 statistic [(observed number of co-occurring fire dates − expected number of fire dates)^2/the expected number of co-occurring fire dates] (*13*) for combinations of fire events (dates) recorded in three or more groves. Thus, although both fire and nonfire events were highly synchronous during the period A.D. 1000 to 1300 (Fig. 1C and Table 1), the high number of multiple-grove fire events was largely due to higher fire frequencies within the groves during this period. A relatively higher synchrony of multiple-grove fire events (that is, higher χ^2 values) was actually observed during lower fire-frequency periods.

Regional synchrony of fire occurrence (and nonoccurrence) was also highest during low fire-frequency periods (Fig. 4), indicating that this pattern is a cross-scale phenomenon. The regional synchrony of fire dates does not indicate continuous burns between the groves; it suggests that large areas burned throughout the region during some years. Thus, during low fire-frequency periods fire-driven vegetation changes were relatively coarse-grain, whereas during high fire-frequency periods they were relatively fine-grain. Twentieth-century landscape patterns reflecting this scaling rule have also been observed in Mexico and Southern California by Minnich (*15*). In these areas, frequent small fires were related to the heterogeneous (fine-grain) structure of chaparral stands south of the border, but infrequent large fires north of the border were related to homogeneous (coarse-grain) chaparral structure. Similar patterns have been shown for ponderosa pine forests of the southwestern United States, where more than 70 years of fire suppression has shifted presettlement fire regimes from frequent low-intensity surface fires to infrequent, but increasingly numerous, large catastrophic crown fires (*16*). The occurrence of regional fire complexes in northern California in 1987, Yellowstone National Park in 1988, and Yosemite National Park in 1990 were caused in part by severe regional droughts, but the accumulation of fuels and changes in forest structure related to fire suppression may have also been involved (*17*). Increasingly synchronized regional fire regimes may be expected in such human-altered forest landscapes subjected to climatic extremes.

Fires have profound effects on ecosystem structure and biodiversity because they alter the availability of habitats in space and time. For example, the coexistence of some early colonizing species with more competitively dominant species depends on the temporal phasing (or synchrony) of disturbances, even if the mean rate of disturbance remains constant (*18*, *4*). Intensities of recent surface burns in sequoia groves were spatially variable (patchy), with important effects on sequoia growth and seedling establishment (*11*). Thus, interpretations of the historical development and current heterogeneity of forest ecosystems require knowledge of both the frequency and related spatial pattern of past disturbances.

Observed heterogeneity at small spatial scales has forced ecologists to accept that the dynamics of most patches are nonequilibrial (*19*). But some have proposed that nonequilibrium patterns within patches might average to equilibrium patterns at larger scales [for example, the "shifting mosaic steady-state" (*20*)]. However, if annual-to-centennial–scale climate patterns synchronize fire histories across spatial scales, then nonequilibrium conditions are likely to exist at all scales (*21*). Over the long term, giant sequoia fire regimes were clearly nonstationary; fire frequencies and sizes constantly changed through time. Hence, it is reasonable to infer that many of the properties and components of these ecosystems (such as biodiversity and rates of nutrient and carbon cycling) were also nonequilibrial. This long-term view supports an ecological paradigm that emphasizes the ubiquity of change in ecosystems, rather than tendencies toward stasis or climax communities (*19*).

REFERENCES AND NOTES

1. A. J. Simard, D. A. Haines, W. A. Main, *Agric. For. Meteorol.* **36**, 93 (1985); T. W. Swetnam and J. L. Betancourt, *Science* **249**, 1017 (1990); T. W. Swetnam and J. L. Betancourt, in *El Niño—Historical and Paleoclimatic Aspects of the Southern Oscillation*, H. F. Diaz and V. Markgraf, Eds. (Cambridge Univ. Press, Cambridge, 1992), pp. 259–270.
2. M. B. Davis and D. B. Botkin, *Quat. Res.* **23**, 327 (1985); J. T. Overpeck, D. Rind, R. Goldberg, *Nature* **343**, 51 (1990); R. E. Keane, S. F. Arno, J. K. Brown, *Ecology* **71**, 189 (1990).
3. T. H. F. Allen and T. B. Starr, *Hierarchy: Perspectives for Ecological Complexity* (Univ. of Chicago Press, Chicago, 1982); R. E. Ricklefs, *Science* **235**, 167 (1987); H. R. Delcourt and P. A. Delcourt, *Landscape Ecol.* **2**, 23 (1988).
4. W. P. Sousa, *Annu. Rev. Ecol. Syst.* **15**, 353 (1984).
5. M. L. Heinselman, in "Proceedings of Conference, Fire Regimes and Ecosystem Properties," H. A. Mooney, T. M. Bonnicksen, N. L. Christensen, J. E. Lotan, W. A. Reiners, Tech. Coords, *Gen. Tech. Rep. WO-26* (U.S. Forest Service, Washington, DC, 1981), pp. 7–57; H. A. Wright and A. W. Bailey, *Fire Ecology—United States and Canada* (Wiley, New York, 1982).
6. D. A. Graybill, in, *Southern California Climate: Trends and Extremes of the Past 2000 Years*, R. Lavenberg, Ed. (Natural History Museum of Los Angeles County, Los Angeles, CA, in press). This reconstruction of total November to March precipitation (A.D. 1060 to 1990) from foxtail pine and giant sequoia ring widths is for California Climate Division 5, which encompasses most of my study area. Precipitation variations (500 to 1970) are also inferred from a lower forest border, bristlecone pine tree-ring–width chronology from the White Mountains, CA (Methuselah Walk area), approximately 50 km east of the Sierra Nevada crest, described in (*7*).
7. V. C. LaMarche Jr., *Science* **183**, 1043 (1974).
8. L. J. Graumlich, *Quat. Res.* **39**, 249 (1993). This reconstruction of mean June to August temperature (A.D. 1000 to 1990), from foxtail pine and western juniper, is for the Grant Grove–Giant Forest area of Sequoia National Park, CA. Growing season temperatures from 500 to 1970 inferred from an upper tree line, bristlecone pine tree-ring–width chronology from the White Mountains, CA (Campito Mountain) is described by V. C. LaMarche Jr. and T. P. Harlan [*J. Geophys. Res.* **78**, 8849 (1973)] and in (*7*).
9. P. W. Rundel, *Madroño* **21**, 319 (1972).
10. M. A. Stokes and T. L. Smiley, *An Introduction to Tree-Ring Dating* (Univ. of Chicago Press, Chicago, 1968); T. W. Swetnam, M. A. Thompson, E. K. Sutherland, *Agric. Handb. 639* (U.S. Forest Service, Washington, DC, 1985). Tree-ring patterns in the fire-scar specimens were cross-dated with existing and recently developed tree-ring–width chronologies [A. E. Douglass, *Climatic Cycles and Tree-Growth: A Study of the Annual Rings of*

Trees in Relation to Climate and Solar Activity (Carnegie Institution of Washington, Washington, DC, 1919); P. M. Brown, M. K. Hughes, C. H. Baisan, T. W. Swetnam, A. C. Caprio, *Tree-Ring Bull.*, in press].
11. R. J. Hartesveldt, *Nat. Hist.* **73**, 12 (1964); N. L. Stephenson, D. J. Parsons, T. W. Swetnam, in *Proceedings—17th Tall Timbers Fire Ecology Conference*, Tallahassee, FL, 18 to 21 May 1989 (Tall Timbers Research Station, Tallahassee, FL, 1991), pp. 321–327; L. Mutch and T. W. Swetnam, in *Proceedings of Symposium on Fire in Wilderness and Park Management, Missoula, Montana*, J. Brown, Tech. Coord., Missoula, MT, 30 March to 1 April 1993 (U.S. Forest Service, Ogden, UT, in press).
12. J. L. Vankat, *Assoc. Am. Geogr. Ann.* **67**, 17 (1977); B. M. Kilgore and D. Taylor, *Ecology* **60**, 129 (1979); H. T. Lewis, "Patterns of Indian Burning in California: Ecology and Ethnohistory," *Ballena Press Anthropol. Pap. No. 1* (Ballena Press, Ramona, CA, 1973).
13. The joint probabilities were the products of the individual probabilities of fire occurrence within each grove, estimated from the observed centennial fire frequencies (annual fire probability equals the number of fires per century divided by 100). This approach is a simplification, because the true fire probabilities were not stationary through time. In addition to the influence of climate change on fire ignition and spread, the accumulation of fuels tends to increase the probability of fire occurrence as a function of time since the last fire. Nevertheless, this test provided a useful measure of how different the observed levels of fire synchrony were among groves, relative to fire synchrony that might have been observed by chance if fire occurrence were random and independent within and among the groves.
14. The observed frequency dependency is not always consistent. Both precipitation and temperature interact to produce droughts and fire responses lasting years to decades. For example, an extreme drought lasting several decades coincided with the largest difference between the regional fire and temperature records during the mid-1200s (Fig. 3). This was one of the driest periods in the tree-ring reconstructions (*6*, *8*), and past lake levels in this region also indicate that the mid-1200s were extremely dry [S. Stine, *Palaeogeogr. Palaeoclimatol. Palaeoecol.* **78**, 333 (1990)].
15. R. A. Minnich, *Science* **219**, 1287 (1983). In this case, the shift to lower fire frequency on the U.S. side of the border, and consequent larger chaparral patches and fires, was primarily a result of fire suppression rather than climate.
16. T. W. Swetnam, in "Proceedings of Symposium on Effects of Fire in Management of Southwestern Natural Resources," S. Krammes, Tech. Coord., *Gen. Tech. Rep. RM-191* (U.S. Forest Service, Fort Collins, CO, 1990), pp. 6–17.
17. N. L. Christensen *et al.*, *BioScience* **39**, 678 (1989).
18. R. Abugov, *Ecology* **63**, 2 (1982); T. E. Miller, *Am. Nat.* **120**, 533 (1982).
19. N. L. Christensen, in *Ecosystem Management for Parks and Wilderness*, J. Agee and D. Johnson, Eds. (Univ. of Washington Press, Seattle, 1989), pp. 62–86; N. L. Christensen, *Forum Appl. Res. Public Policy* **4**, 46 (1989).
20. F. H. Bormann and G. E. Likens, *Pattern and Process in a Forested Ecosystem* (Springer-Verlag, New York, 1979).
21. W. H. Romme, *Ecol. Monogr.* **52**, 199 (1982); D. H. Knight, in *Landscape Heterogeneity and Disturbance*, M. G. Turner, Ed. (Springer-Verlag, New York, 1987), pp. 59–83.
22. I thank the many assistants, students, National Park Service personnel, California Department of Forestry personnel, and volunteers who contributed by carrying out field, shop, and laboratory tasks, foremost among whom were C. H. Baisan, P. M. Brown, A. C. Caprio, and R. Touchan of the Laboratory of Tree-Ring Research, University of Arizona; I also thank J. L. Betancourt, L. J. Graumlich, M. K. Hughes, D. J. Parsons, N. L. Stephenson, and two anonymous reviewers for commenting on and editing the manuscript. Supported by Sequoia, Kings Canyon, and Yosemite National Parks and National Park Service Global Change Program Cooperative Agreements, Department of the Interior 8018-1-0002 and 8032-1-0002.

11 June 1993; accepted 30 August 1993

Controls on Geyser Periodicity

S. E. Ingebritsen* and S. A. Rojstaczer

Geyser eruption frequency is not constant over time and has been shown to vary with small ($\leq 10^{-6}$) strains induced by seismic events, atmospheric loading, and Earth tides. The geyser system is approximated as a permeable conduit of intensely fractured rock surrounded by a less permeable rock matrix. Numerical simulation of this conceptual model yields a set of parameters that controls geyser existence and periodicity. Much of the responsiveness to remote seismicity and other small strains in the Earth can be explained in terms of variations in permeability and lateral recharge rates.

In contrast to steady surface-discharge features such as fumaroles and hot springs, which are common in regions with active geothermal systems, periodic geysers are rare (*1*). Most occur in areas where the water table is near the land surface and hydrostatic boiling-point conditions are present to depths of about 200 m. Geyser systems are commonly described in terms of a shallow low-permeability seal (*1*) or constriction (*2*) underlaid by a chamber that periodically erupts a steam-water mixture (*1–3*) (Fig. 1A). In this model, eruption magnitude and frequency are governed by chamber and seal geometry.

To examine geyser periodicity in a quantitative fashion, we invoke a modification of the chamber model. We approximate the chamber as a zone of fractured rock (Fig. 1B). Instead of being constricted only at the top of the chamber, flow is controlled everywhere in the fracture zone by fracture permeability. The fluid-saturated fracture zone is a permeable, compliant column surrounded by less permeable and less compliant rock. We determined a set of parameters that controls geyser periodicity by numerical simulation of the fracture-zone model.

Geyser eruption frequency is not constant over time (*4*). For most geysers, eruption frequency is irregular, especially when other geysers exist nearby (*5*). Even famously regular geysers such as Old Faithful of Yellowstone exhibit variations in their eruption intervals (*6*). Over various time scales, eruption interval has been shown to vary with small strains (typically less than 1 μ-strain) induced by variations in atmospheric loading, Earth tides, and seismic events (*4*, *7–8*). Much of this responsiveness to small strains should be controlled by changes in model parameters.

We investigate geyser behavior using a mathematical model of heat and mass transport in permeable media. The flow of fluid and heat is described by coupled, multiphase mass- and energy-balance equations (*9*)

$$\partial (n\rho_f)/\partial t - \nabla \cdot [\bar{\bar{k}} k_{rs}\rho_s/\mu_s \cdot (\nabla P - \rho_s g \nabla D)] - \nabla \cdot [\bar{\bar{k}} k_{rw}\rho_w/\mu_w \cdot (\nabla P - \rho_w g \nabla D)] - q_m = 0 \quad (1)$$

and

$$\partial/\partial t[n\rho_f h_f + (1-n)\rho_r h_r] - \nabla \cdot [\bar{\bar{k}} k_{rs}\rho_s h_s/\mu_s \cdot (\nabla P - \rho_s g \nabla D)] - \nabla \cdot [\bar{\bar{k}} k_{rw}\rho_w h_w/\mu_w \cdot (\nabla P - \rho_w g \nabla D)] - \nabla \cdot [K_m(\partial T/\partial P)_h \nabla P + K_m (\partial T/\partial h)_p \nabla h] - q_h = 0 \quad (2)$$

respectively, where D is depth, g is gravitational acceleration, h is enthalpy, $\bar{\bar{k}}$ is the

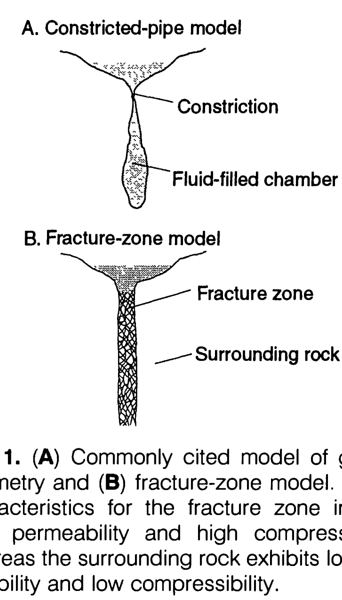

Fig. 1. (**A**) Commonly cited model of geyser geometry and (**B**) fracture-zone model. In (B), characteristics for the fracture zone include high permeability and high compressibility, whereas the surrounding rock exhibits low permeability and low compressibility.

S. E. Ingebritsen, U.S. Geological Survey, Menlo Park, CA 94025.
S. A. Rojstaczer, Department of Geology, Duke University, Durham, NC 27708.

*To whom correspondence should be addressed.